Since the energization process to form SiH_3Cl^* is chemical activation by insertion of SiH_2 into HCl, it is not likely that there is any significant temperature coefficient of k_{-4} and k_7. The collisional deactivation rate constant k_8 is not likely to be temperature dependent, it generally being taken as being the rate constant for molecular collisions. Therefore, we conclude that the observed temperature dependence, or lack of it, seen in Figures 3 and 4 reflects the fact that under our conditions $E_4 \approx E_3$. E_3 has been reported[13] to be 1.3 kcal/mol.

(b) Formation of Dichlorosilane and Trichlorosilane. In view of the facts that SiH_2 is the predominant reactive species produced in the infrared multiphoton decomposition of SiH_4[2-5] and that SiH_2Cl_2 and $SiHCl_3$ are formed simultaneously with SiH_3Cl and Si_2H_6, the most feasible mechanism for formation of dichlorosilane and trichlorosilane is as shown in (13)–(17). The very small

$$SiHCl + HCl \rightleftarrows SiH_2Cl_2^* \quad (13)$$

$$SiH_2Cl_2^* \rightarrow SiCl_2 + H_2 \quad (14)$$

$$SiH_2Cl_2^* + M \rightarrow SiH_2Cl_2 + M \quad (15)$$

$$SiCl_2 + HCl \rightleftarrows SiHCl_3^* \quad (16)$$

$$SiHCl_3^* + M \rightarrow SiHCl_3 + M \quad (17)$$

amounts of what we believe to be SiH_3SiH_2Cl most probably result from insertion of SiHCl into SiH_4, as shown by (18) and (19).

$$SiHCl + SiH_4 \rightleftarrows Si_2H_5Cl^* \quad (18)$$

$$Si_2H_5Cl^* + M \rightarrow Si_2H_5Cl + M \quad (19)$$

$SiCl_2$ will most likely also insert into SiH_4, (20), although we have not detected the ultimate product of this reaction.

$$SiCl_2 + SiH_4 \rightleftarrows Si_2H_4Cl_2^* \quad (20)$$

A standard kinetic treatment of the mechanism leads to the following expressions for the rate ratios $R(SiH_2Cl_2)/R(SiH_3Cl)$ and $R(SiHCl_3)/R(SiH_2Cl_2)$:

$$\frac{R(SiH_2Cl_2)}{R(SiH_3Cl)} = \left(\frac{k_7k_{15}/k_8}{k_{-13} + k_{14} + k_{15}[M]}\right)\frac{(k_{13}/k_{18})([HCl]/[SiH_4])}{1 + (k_{13}/k_{18})([HCl][SiH_4])} \quad (21)$$

$$\frac{R(SiHCl_3)}{R(SiH_2Cl_2)} = \left(\frac{k_{14}k_{17}/k_{18}}{k_{-16} + k_{17}[M]}\right)\frac{(k_{16}/k_{20})([HCl]/[SiH_4])}{1 + (k_{16}/k_{20})([HCl]/[SiH_4])} \quad (22)$$

We have already noted, e.g., (9) and (12), that unimolecular decomposition of the chemically activated monochlorosilane appears to be very rapid relative to collisional deactivation in the pressure regime studied. The same is very likely true for $SiH_2Cl_2^*$ and $SiHCl_3^*$, since the number of internal degrees of freedom is the same. Therefore, we assume $(k_{-13} + k_{14}) >> k_{15}[M]$ and $k_{-16} >> k_{17}[M]$. With these assumptions, we see that for experiments at constant $[HCl]/[SiH_4]$, the rate ratios in (21) and (22) should be independent of third-body concentration or, equivalently, of total pressure. That this is true within experimental error may be seen in Figure 7, in which the ratios $R(SiH_2Cl_2)/R(SiH_3Cl)$ and $R(SiHCl_3)/R(SiH_3Cl)$ are plotted vs. the partial pressure of CH_4.

On the other hand, for experiments at constant total pressure, but increasing $[HCl]/[SiH_4]$, the rate ratios should increase in a linear fashion. As in Figure 8, this prediction is also born out by the experimental facts. It is to be seen from Figure 8 that the plots do not go through the origin as predicted by (21) and (22). We believe this is due to the presence of very small amounts of chlorosilanes as impurities in the silane and the intercepts of Figure 8 simply reflect the ratios of these impurities. The impurities arise, of course, from the synthesis of silane via the reduction of silicon tetrachloride.

Finally, the linearity seen in Figure 8 for $[HCl]/[SiH_4]$ up to a value of 1.0, suggests that

$$k_{13}/k_{18} << 1 \qquad k_{16}/k_{20} << 1$$

This effect of chlorine substitution in reducing silylene reactivity toward insertion into the H–Cl bond is in accord with the reactivity order reported for insertion into Si–H bonds.[23]

Acknowledgment. This is work was supported by Contract No. DE-AS02-76ER03416 with the U.S. Department of Energy.

Registry No. SiH_4, 7803-62-5; HCl, 7647-01-0; H_2, 1333-74-0; Si_2H_6, 1590-87-0; SiH_3Cl, 13465-78-6; SiH_2Cl_2, 4109-96-0; $SiHCl_3$, 10025-78-2; Si_3H_8, 7783-26-8; Si_2H_5Cl, 14565-98-1; Si, 7440-21-3.

Metal Cluster Electronic and EPR Properties: SCF–Xα–SW Prediction of the Magnetogyric (g) and Superhyperfine Tensors of Trigonal-Bipyramidal Charged Silver Clusters Ag_5^{q+} (where q = 2 or 4)

Geoffrey A. Ozin,* Saba M. Mattar,* and Douglas F. McIntosh

Contribution from the Lash Miller Chemistry Department, University of Toronto, Toronto, Ontario, Canada M5S 1A1. *Received November 25, 1983*

Abstract: The effect of gradually depleting valence electronic charge from a model, neutral pentaatomic ligand-free cluster, Ag_5^0, is investigated by using the SCF–Xα–SW method. Specifically, electronic ground- and excited-state wave functions, charge distributions, and eigenvalues are calculated for trigonal-bipyramidal Ag_5^{q+} (q = 0–4) clusters. First ionization potentials for q = 0–4 and excitation energies for q = 0, 2, and 4 are computed and discussed in terms of optical spectroscopic trends as a function of charge on the cluster. Isotropic and anisotropic magnetogyric (g) and hyperfine tensor components are calculated from first principles using the SCF–Xα–SW–MO charge and spin-density distributions for isotopically pure $^{109}Ag_5^{q+}$ for q = 2 and 4. Trends in their EPR parameters and predicted spectra as a function of charge on the cluster are discussed. Calculations of this type are expected to be useful for deciphering optical and EPR spectra of neutral and/or cationic silver clusters entrapped in, for example, rare gas solid, zeolite, or aqueous glassy matrices.

Interest in ligand-free metal clusters has grown steadily over the past decade.[1] A major trend has been an attempt to correlate the structure and bonding of the low nuclearity clusters with their spectroscopic properties, ultimately to gain an understanding of

0002-7863/84/1506-7765$01.50/0

Table I. Geometric Parameters for the Ag_5^{q+} Molecules

atom	atom type	x^a	y^a	z^a	radius[a]	α
1	out	0.00	0.00	0.00	7.246 844 8	0.701 45
2	Ag_1	3.142 244 20	0.00	0.00	2.721 263 3	0.701 45
3	Ag_2	0.00	0.00	4.443 804 30	2.803 040 5	0.701 45
4	Ag_1	−1.571 122 10	2.721 263 30	0.00	2.721 263 3	0.701 45
5	Ag_1	−1.571 122 10	−2.721 263 30	0.00	2.721 263 3	0.701 45
6	Ag_2	0.00	0.00	−4.443 804 30	2.803 040 5	0.701 45

[a] Coordinates and radii given as multiples of the Bohr radius of the hydrogen atom.

their reactivity and potential role as catalysts.[2] The molecular properties of such few-atom clusters, which may in principle be predicted by means of ab initio Hartree–Fock calculations employing configuration interaction, include electronic and nuclear magnetic resonance, electronic absorption, ionization potentials, geometry, bond energies, and the like. In order for an ab initio calculation to adequately represent, for example, the EPR properties of a ligand-free metal cluster, one would have to at least utilize one-electron double-ζ minimum basis sets. Such calculations are costly on computer time. However, for properties that depend on one-electron operators and wave functions, such as ionization potentials, isotropic EPR, and NMR Hamiltonian parameters, the Xα multiple scattering molecular orbital technique of Slater and Johnson[3] may be used with appreciable savings of computational time.[4]

There has been little theoretical work reported concerning the prediction of metal cluster EPR properties. Only the EPR spectra of alkali-metal clusters, such as K_3, have been calculated from first principles.[5] In the case of K_3, several approximations regarding the prediction of the EPR spectral line shapes were made. These included the neglect of the anisotropic magnetogyric (**g**) and (super)hyperfine tensor (**A**) components. In the case of a potassium atom, this is justifiable because the effective spin–orbit interaction is small. Even so, there are noticeable differences between theory and experiment for K_3. Although the predicted EPR stick spectrum for K_3 was presented, no elaborate formulation of the **g** and **A** tensors was given.[5]

There have recently been a number of publications dealing with the theory of **g** and **A** tensors as predicted by Xα techniques.[6] In all of these calculations the problem consisted of a transition-metal center surrounded by organic ligands (e.g., metalloporphyrins and metallocenes). This amounted to solving the problem of a single center possessing appreciable spin–orbit coupling with the normal ligand-field approximations applied to the **g** and **A** tensors. In these cases the Xα calculation serves as a refinement to the already intuitively predictable chemical properties of the molecule.

In contrast, the a priori prediction of the EPR spectra arising from a ligand-free transition-metal cluster is not easy to predict without some prior knowledge of the electronic structure and molecular orbital charge distribution of the cluster. Furthermore, the multicenter nature of the cluster and the delocalization of the cluster valence electron(s) over more than one metal atom with comparable spin–orbit coupling constants renders the estimation of the **g** and **A** tensors difficult. Although extensive delocalization of an unpaired electron over more than a single atom in a molecule is also encountered in organic-free radicals,[7] one finds that the relatively small spin–orbit coupling constants of atoms like hydrogen, carbon, nitrogen, and oxygen do not induce a very large anisotropy into the **g** and **A** tensors. However, in the case of transition-metal clusters without ligands the spin–orbit coupling constants can be at least 2 orders of magnitude larger than those of H, C, N, and O. Thus the resulting metal-cluster EPR spectrum is not readily predictable.

Table II. Predicted First Ionization Energies of the Ag_5^{q+} Molecules

molecule	HOMO	term symbol	1st ionization potential, eV
Ag_5^0	$(6e')^1$	$^2E'$	6.45
Ag_5^{1+}	$(3a_2'')^2$	$^1A_1'$	11.21
Ag_5^{2+}	$(3a_2'')^1$	$^2A_2''$	15.62
Ag_5^{3+}	$(4a_1')^2$	$^1A_1'$	23.18
Ag_5^{4+}	$(4a_1')^1$	$^2A_1'$	27.98

In this study the SCF–Xα–SW–MO method is used to predict the electronic properties, effective spin-Hamiltonian parameters, charge, and spin-density distributions for isotopically pure $^{109}Ag_5^{q+}$ (q = 2 or 4). This choice of metal cluster was predicated on recent discoveries of cationic silver clusters entrapped in the α and β cages of silver-exchanged sodium zeolites X, Y, and A[8] as well as in γ-irradiated frozen aqueous glasses of silver salts,[9] having nuclearities in the range 2–6. As the optical spectrum of Ag_5^0 isolated in rare gas solids is known[10] and the EPR spectrum of Ag_5^0 isolated in cryogenic adamantane and cyclohexane matrices is consistent with that of a trigonal bipyramid[11] (subject to a probable dynamic Jahn–Teller distortion), the structure selected for the Ag_5^{2+} and Ag_5^{4+} clusters of the present theoretical study was also chosen to be that of a trigonal bipyramid with D_{3h} symmetry.

Calculational Details

The electronic structure calculations were performed using the self-consistent field–Xα–scattered wave (SCF–Xα–SW) theory,[3,12] the methodology of which has been described elsewhere.[13] This was accomplished with a modified version of the original set of programs by Johnson and Smith in double precision mode. α parameters were taken from the tabulations of Schwarz.[14] The α values for the outer sphere and the intersphere regions were set to the valence-electron weighted average of those for the constituent atoms. The magnitudes of the atomic sphere radii were derived by Norman's method.[15] Partial wave expansions were included for values of l up to 4 for the outer sphere ("out") and

(1) Ozin, G. A.; Mitchell, S. A. *Angew. Chem.*, Int. *Ed. Engl.* **1983**, *22*, 674–694 and references cited therein.
(2) Baetzold, R. C.; Hamilton, J. F. *Prog. Solid State Chem.* **1983**, *15*, 1 and references cited therein.
(3) Johnson, K. H.; Smith, F. C., Jr. *Phys. Rev. B: Solid State* **1972**, *5*, 831. Slater, J. C.; Johnson, K. H. *Ibid.* **1972**, *5*, 844.
(4) Messmer, R. P. In "The Nature of the Surface Chemical Bond"; Rhodin, T., Ertl, G., Eds.; North-Holland: Amsterdam, 1982. Case, D. A.; Cook, M.; Karplus, M. *J. Chem. Phys.* **1980**, *73*, 3294.
(5) Dietz, E. R. *Phys. Rev. A* **1981**, *23*, 751.
(6) Case, D. A.; Karplus, M. *J. Am. Chem. Soc.* **1977**, *99*, 6182. Weber, J.; Goursot, A.; Pénigault, E.; Ammeter, J. H.; Bachmann, J. *J. Am. Chem. Soc.* **1982**, *104*, 1491. Sontum, S. F.; Case, D. A. *J. Phys. Chem.* **1982**, *86*, 1596.
(7) Stone, A. J. *Mol. Phys.* **1963**, *6*, 509; *Ibid.* **1963**, *7*, 31.
(8) Ozin, G. A.; Hugues, F.; Mattar, S. M.; McIntosh, D. F. *J. Phys. Chem.* **1983**, *87*, 3445; In "Intrazeolite Chemistry" Stucky, G. D., Dwyer, F. G., Eds.; American Chemical Society: Washington, DC, 1983; ACS Symp. Ser. No. 218, p 409 and references cited therein.
(9) Symons, M. C. R.; Forbes, C. E. *Mol. Phys.* **1974**, *27*, 467.
(10) Ozin, G. A.; Mitchell, S. A. *J. Phys. Chem.* **1984**, *88*, 1425.
(11) Howard, J. A.; Preston, K. F.; Sutcliffe, R.; Mile, B.; Tse, J. S. *J. Phys. Chem.* **1983**, *87*, 2268.
(12) Weinberger, P.; Schwarz, K. *Int. Rev. Sci.: Phys. Chem., Ser. Two 1975–1976* **1975**, *1*, 255. Johnson, K. H. *Adv. Quantum Chem.* **1973**, *7*, 143. Rösch, N. *NATO Adv. Study Inst. Ser., Ser. B* 1977, *24*, 1. Connoly, J. W. D.; "Semiempirical Methods of Electronic Structure Calculations"; Segal, G. A.; Ed.; Plenum Press: New York, 1979; Part A, Techniques, p 105. Slater, J. C. "The Calculation of Molecular Orbitals"; Wiley: New York, 1979.
(13) McIntosh, D. F.; Ozin, G. A.; Messmer, R. P. *Inorg. Chem.* **1980**, *19*, 3321.
(14) Schwarz, K.; *Phys. Rev. B: Solid State* **1972**, *5*, 2466. Schwarz, K.; *Theor. Chim. Acta* **1974**, *34*, 225.
(15) Norman, J. G., Jr. *J. Chem. Phys.* **1974**, *61*, 4630. Norman, J. G., Jr. *Mol. Phys.* **1976**, *31*, 1191.

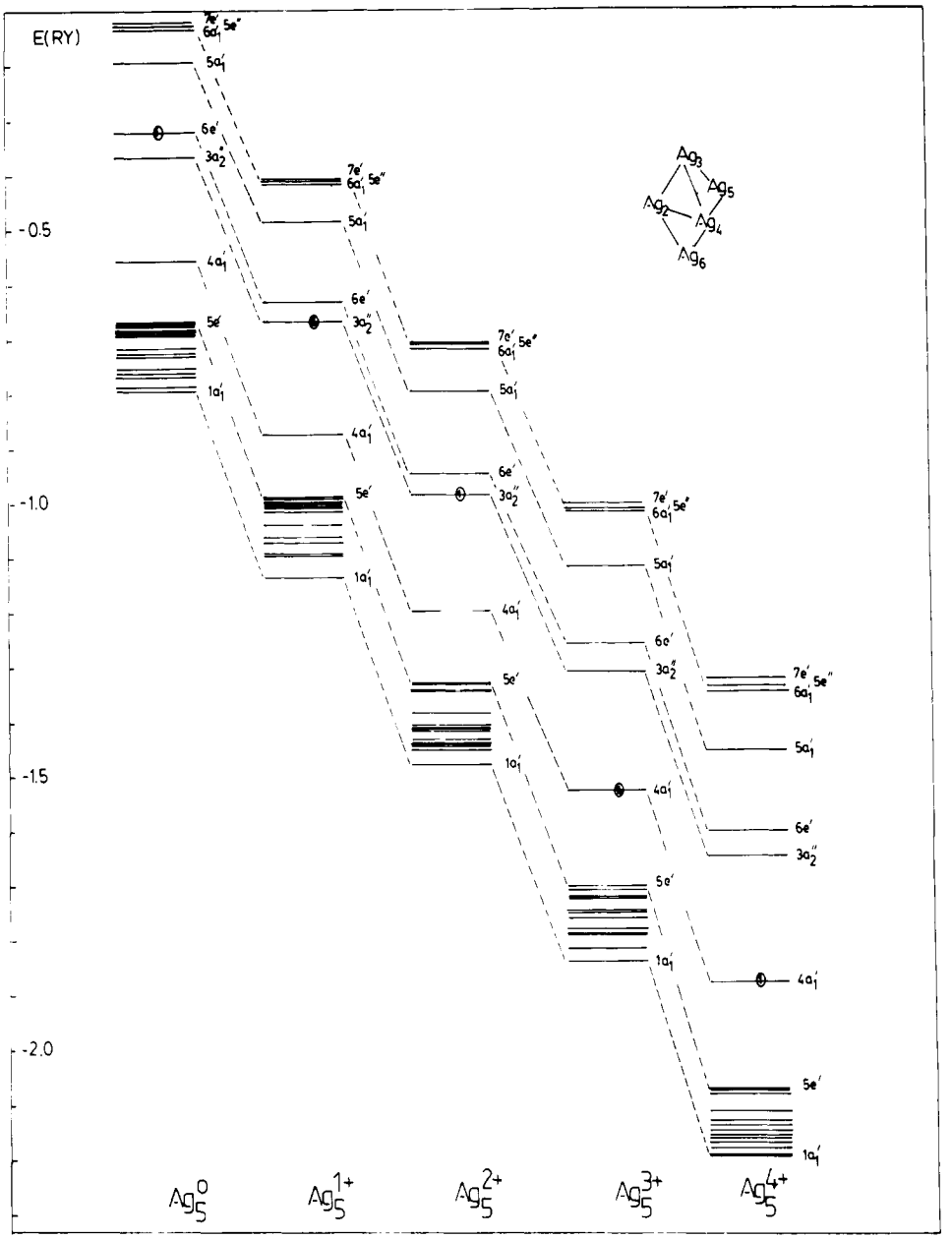

Figure 1. Energy level diagrams for Ag_5^{q+} (where q = 0, 2, or 4). Note energies are expressed in Rydberg units.

up to 2 for the two different types of silver atoms ("Ag_1" and "Ag_2").

A trigonal-bipyramidal geometry (D_{3h} symmetry) was adopted for the silver clusters. Structural details are given in Table I. The internuclear distances were assumed to be identical with those of the bulk metal (i.e., 2.88 Å). The ground-state electronic structures of the cationic molecular clusters were obtained by initially determining that of the neutral molecule followed by the successive removal of half an electron, from each converged species, until the $Ag_5^{4.5+}$ molecule was reached. In this way, not only were convergence problems minimized but the steady depletion of charge from a given molecular system, in which the geometrical parameters were held constant, could be studied more easily. In addition, the determination of the ground-state structures of the clusters with half-integral charge immediately afforded an estimate of the first ionization potential of the neutral and integrally charged species, through the use of the transition-state model.[3,12] In this case, the absolute value of the energy of the highest occupied molecular orbital (HOMO) of the $Ag_5^{(q+1/2)+}$ species would be equal to the first ionization potential of the Ag_5^{q+} molecule. These values are collected in Table II. It should be emphasized that these values are actually proportional to and not exactly equal to the expected experimental quantities.

General Electronic and Bonding Considerations. The energy level diagrams for the Ag_5^{q+} species are illustrated in Figure 1.[16] Focusing attention, initially, on the neutral molecule, we may determine the symmetry types of the bonding molecular orbitals of Ag_5^0 by making the assumption that the basic electronic network of the cluster may be represented by the nine nearest-neighbor, "σ-like", internuclear bonds. Although this is an oversimplification of the true bonding scheme, it will provide us with a starting point from which one may understand the bonding and spectroscopy for these clusters.

Simple group theoretical considerations lead to the prediction that the reducible representation formed from these nine silver–silver interactions may be decomposed into the following linear combination of irreducible representations:

$$2A_1' + 2E' + 1A_2'' + 1E''$$

On examining the partial wave analyses and contour diagrams for neutral Ag_5^0, one may readily determine that the most significant metal–metal interactions do indeed result from molecular

(16) The partial wave analysis for the ground- and excited-state spin-restricted calculations of the molecular clusters Ag_5^{q+} (where q = 0–4) are available from the authors on request.

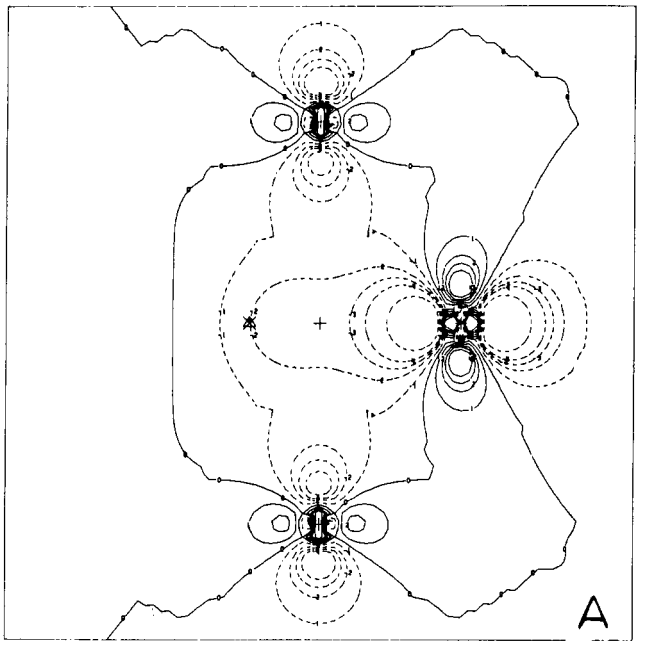

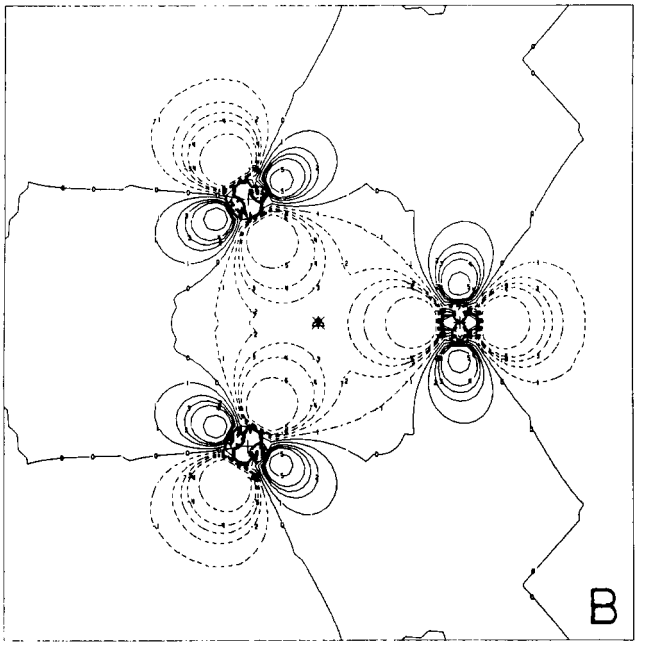

Figure 2. Wave-function contour diagrams for the $1a_1'$ molecular orbital of neutral Ag_5^0. (A) Plot of the *xz* plane, (B) plot of the *xy* plane. Note that positive wave-function contours are indicated by a solid line while negative wave-function contours are given by dashed lines. Contour specifications: (1) 0.03, (2) 0.06, (3) 0.08, (4) 0.10, and (5) 0.15 in units of $(\text{electron}/a_0^3)^{1/2}$. The "0" contours represent nodal surfaces.

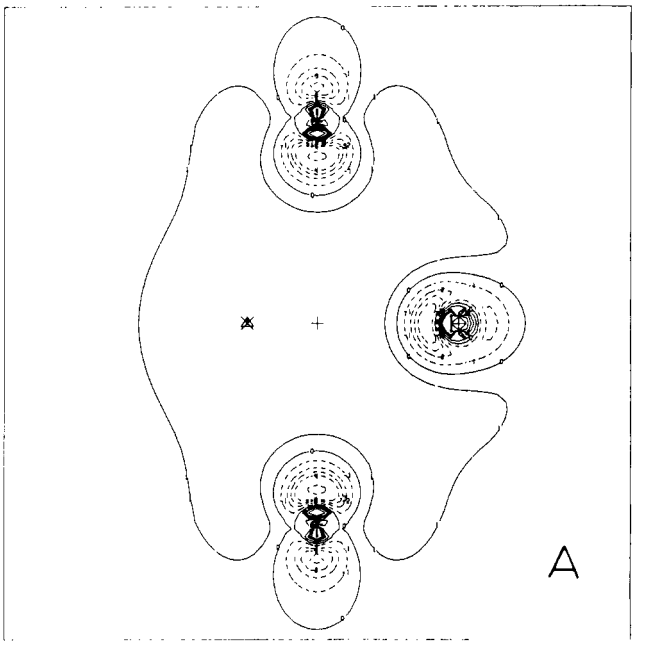

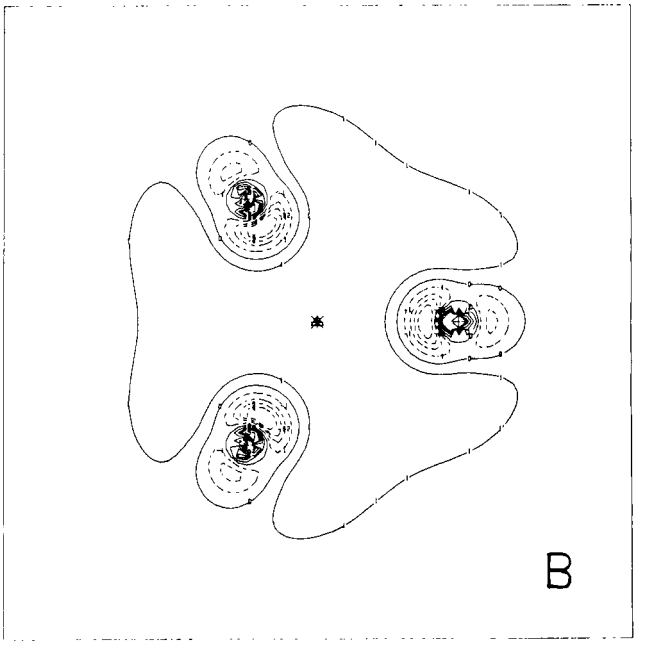

Figure 3. Wave-function contour diagrams for the $4a_1'$ molecular orbital of neutral Ag_5^0. (A) Plot of the *xz* plane, (B) plot of the *xy* plane. See Figure 2 caption for contour specifications.

orbitals of these symmetry types, namely, $1a_1'$ (Figure 2), $4a_1'$ (Figure 3), $1e'$, $2e'$, $1a_2''$ (Figure 4), and $1e''$. Only three contour diagrams are included for illustrative purposes.

Interestingly, apart from the $4a_1'$ level, all of the molecular orbitals of this group result almost exclusively from the overlap of the 4d atomic orbitals of the silver atoms. The $4a_1'$ level is composed primarily of 5s valence atomic orbitals. Accordingly, their combination results in a rather diffuse molecular orbital with very little internuclear charge density as shown in Figure 3. Although one might have anticipated that the lower lying 4d-like molecular orbitals would have behaved as corelike, noninteracting levels and would therefore not be expected to contribute significantly to the overall bonding scheme in the cluster,[17] this in fact is not entirely the case as seen by examination of the wave-function contour plot of the $1a_1'$ molecular orbital shown in Figure 2. Clearly, both the $4a_1'$ and $1a_1'$ orbitals contribute to the overall cluster bonding scheme. Quantification of the relative importance of each, however, is beyond the scope of the present study.

At energies just slightly higher than those of the eight 4d-like bonding molecular orbitals lie a set of molecular levels, again almost exclusively 4d-like in character, which might be described as being nonbonding or only slightly interactive in nature ($2a_1'$, $3a_1'$, $1a_2'$, $3e'$, $4e'$, $5e'$, $1a_1''$, $2a_2''$, $2e''$, $3e''$, and $4e''$). A selective set illustrating this orbital type is presented in Figures 5–7. With the former eight and latter 17 4d-like combinations of atomic orbitals, we have essentially accounted for the 25 atomic 4d orbitals from the constituent atoms that form a major part of the basis set. It should be noted, however, that the separation of these 4d-like molecular orbitals into two sets is somewhat arbitrary and should not be taken too literally since the bonding in a molecular metal cluster of this type would be expected to exhibit multicenter interactions between nearest neighbors as well as next-to-near-

(17) Ozin, G. A.; Huber, H.; McIntosh, D. F.; Mitchell, S. A.; Norman, J. G., Jr.; Noodleman, L. *J. Am. Chem. Soc.* **1979**, *101*, 3504.

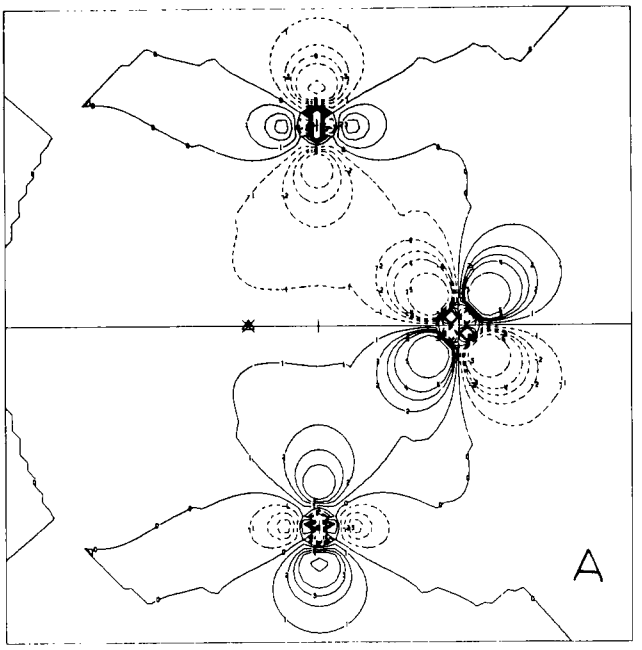

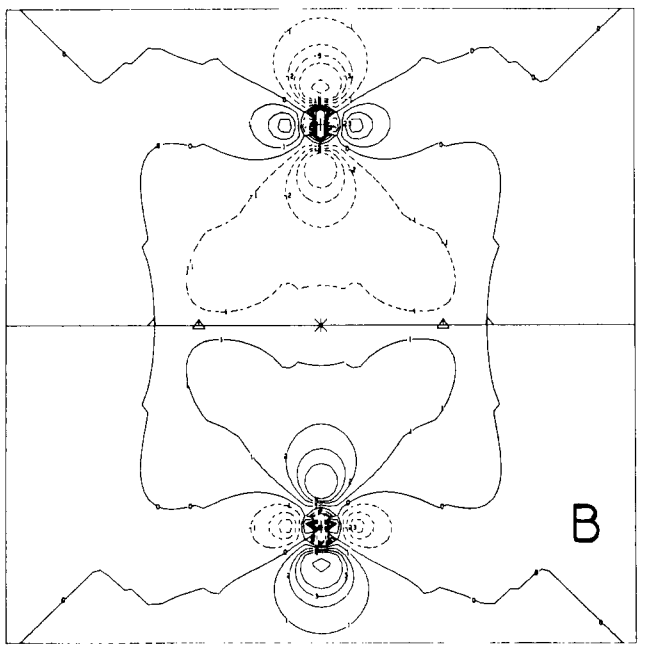

Figure 4. Wave-function contour diagrams for the $1a_2''$ molecular orbital of neutral Ag_5^0. (A) Plot of the *xz* plane, (B) plot of the *yz* plane. Note, the *xy* is a nodal plane. See Figure 2 caption for contour specifications.

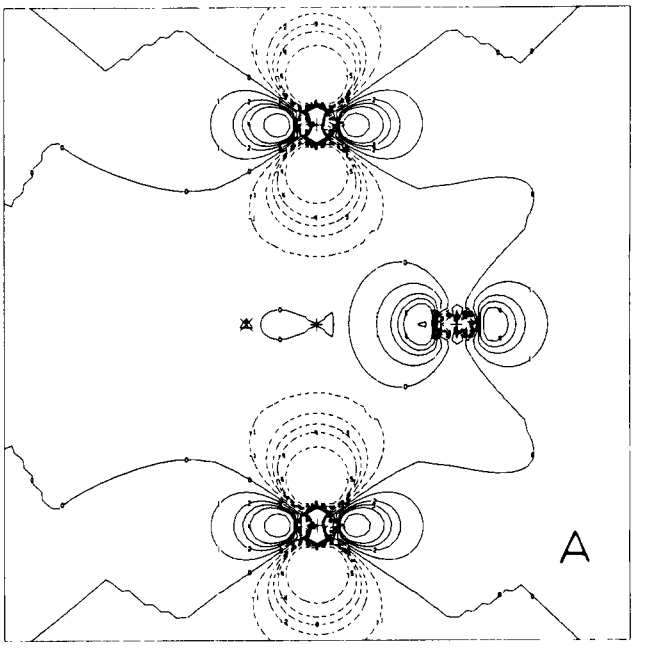

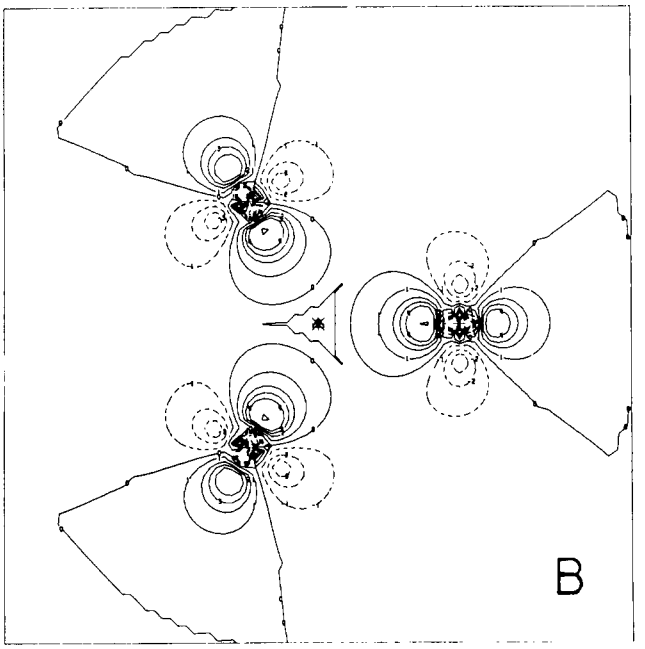

Figure 5. Wave-function contour diagrams for the $3a_1'$ molecular orbital of neutral Ag_5^0. (A) Plot of the *xz* plane, (B) plot of the *xy* plane. See Figure 2 caption for contour specifications.

est-neighbor atoms. As such, all 25 molecular combinations must be considered in a general molecular orbital description involving the 4d orbitals of the contributing atoms.

The remaining molecular orbitals ($5a_1'$, $6a_1'$, $6e'$, $7e'$, $3a_2''$, and $5e''$), as well as the previously mentioned $4a_1'$, tend largely to be derived from the more diffuse 5s and 5p valence atomic orbitals of the silver atoms and, accordingly, are rather diffuse as well. Figure 8 illustrates the highest occupied molecular orbital (HOMO) of the neutral molecule ($6e'$). It should be clear from this figure that this orbital (one component of a doubly degenerate representation) is composed primarily of 5s/5p hybrid atomic orbitals. Thus, the neutral Ag_5^0 trigonal-bipyramidal cluster is expected to have a $^2E'$ ground electronic state and should be subject to a Jahn–Teller distortion.[18] This prediction is borne out by recent ESR measurements for Ag_5^0 in hydrocarbon matrices at 77 K.[11]

As charge is successively removed from the HOMO's of these molecules, the systems experience a general relaxation effect, as best shown by the downward trend in the eigenvalues illustrated in Figure 1. The HOMO's and the resulting molecular electronic term symbols for these species are also summarized in Table II. Clearly, one would expect Ag_5^0, Ag_5^{2+}, and Ag_5^{4+} to be paramagnetic whereas Ag^{1+} and Ag_5^{3+} would be expected to be diamagnetic. Since electronic charge is being progressively removed from molecular orbitals that are relatively delocalized and diffuse, the downward shift of eigenvalues is approximately linear with energy gaps remaining relatively constant. Moreover, there are no dramatic differences between the partial wave analyses of the ground-state electronic configurations of the neutral cluster and the cationic species. A comparison of the analyses of four representative molecular levels for neutral Ag_5^0 and cationic Ag_5^{4+} is presented in Table III, for illustrative purposes. Included in this tabulation are the various HOMO levels ($6e'$, $3a_2''$, $4a_1'$) as

(18) Engleman, R. "The Jahn Teller Effect in Molecules and Crystals"; Wiley: New York, 1972.

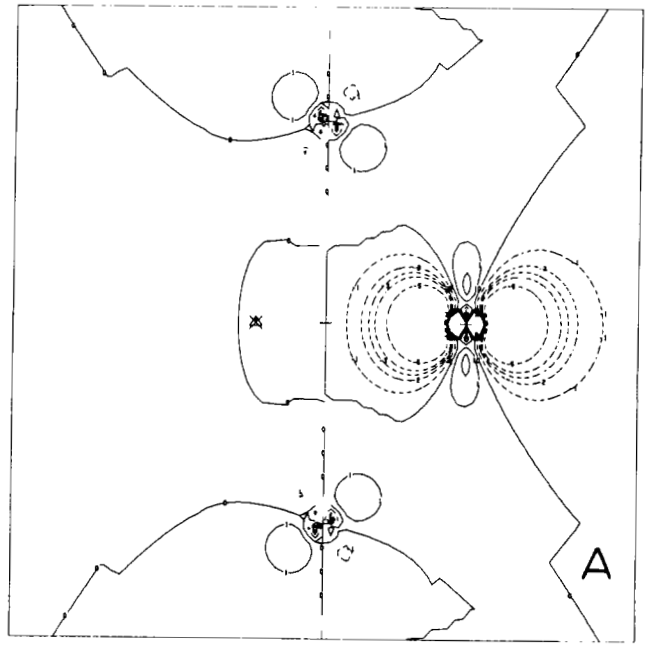

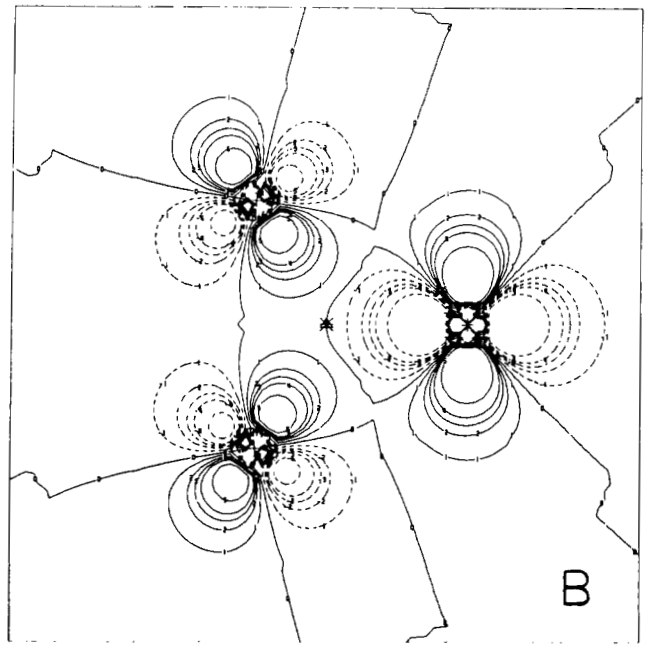

Figure 6. Wave-function contour diagrams for the 3e′ molecular orbital of neutral Ag_5^0. (A) Plot of the *xz* plane, (B) plot of the *xy* plane. See Figure 2 caption for contour specifications.

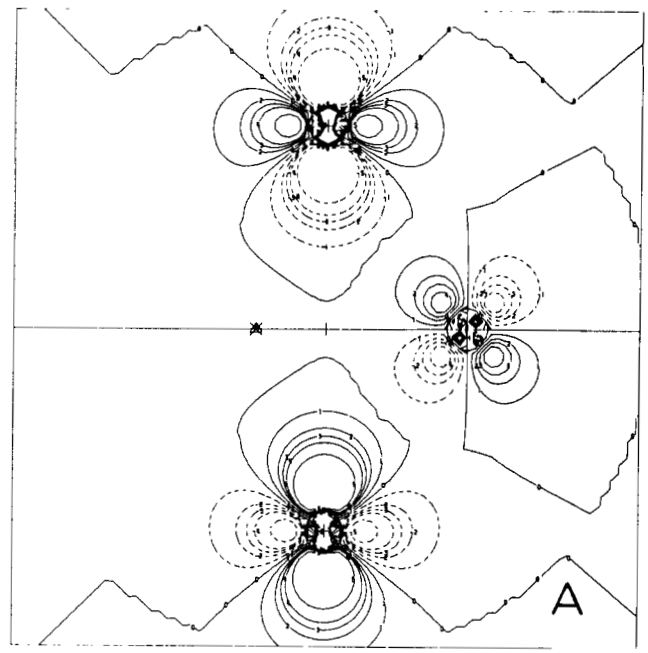

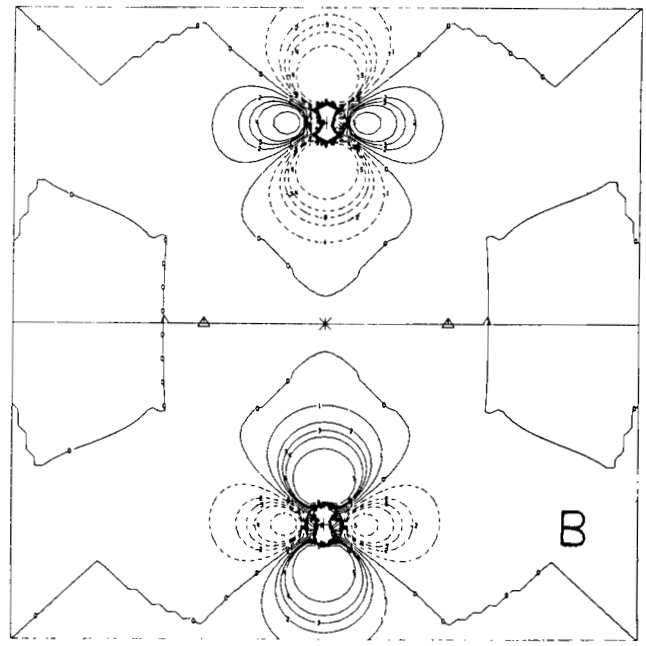

Figure 7. Wave-function contour diagrams for the $2a_2''$ molecular orbital of neutral Ag_5^0. (A) Plot of the *xz* plane, (B) plot of the *yz* plane. Note that *xy* is a nodal plane. See Figure 2 caption for contour specifications.

well as the most stable molecular level ($1a_1'$). For convenience, the partial wave analyses of these levels for the other cationic structures may be appropriately interpolated from these values.[16]

As noted earlier, a simplified valence-bond description of the electronic structures of these molecules would begin with the supposition that the 4d valence atomic orbitals of silver would behave as corelike levels and that only the 5s and 5p valence atomic orbitals would participate to any significant degree in the overall bonding scheme. In this context, Ag_5^{4+} would be envisaged as a pentaatomic cluster held together by a single electron delocalized over the entire structure. In light of the molecular orbital comparisons in Table III, it is noteworthy that, as charge is successively extracted from each cluster, the amount of intersphere charge decreases in a monotonic fashion. Thus, we would expect each molecular orbital to contract in size, even though the relative combinations of basis atomic orbitals remain approximately constant. Therefore, as we tend toward more positively charged clusters, we would expect the bonding, 4d-like molecular levels to overlap to a progressively lesser extent and thereby decrease in importance. Conversely, the initially diffuse $4a_1'$ molecular orbital, formed from the overlap of 5s/5p hybrid orbitals, will contract as well, thereby concentrating progressively greater electronic charge density into the internuclear regions of space. Thus, we would expect the 5s/5p-like bonding levels to increase in importance, as the overlap of the 4d-like levels tended to be less significant. The wave-function contour diagrams for the relevant molecular orbitals of Ag_5^0, Ag_5^{2+}, and Ag_5^{4+} are found to support this contention. The aforementioned bonding description that ignored 4d–4d interactions may be viewed as an extreme interpretation of this trend.

It is evident from the partial wave analyses and the 4d band width of all of these molecules, that the 4d-like levels play a small but not insignificant role in the overall bonding scheme. In fact, as charge is depleted from these molecules, it is the orbital populations of the molecular levels made up of 5s/5p hybrid orbitals that are diminished. The filled 4d-like levels remain untouched in this successive ionization process. It would obviously be in-

Table III. Energies, Percent Charges, and Partial Wave Analyses for Several Molecular Levels of Ag_5^0 and Ag_5^{4+}

molecular orbital		Ag_5^0			Ag_5^{4+}		
		outer	Ag_1	Ag_2	outer	Ag_1	Ag_2
$1a_1'$	% charge	0.10	27.93	5.32	0.04	29.54	3.46
	s	15.95	2.83	2.31	14.84	1.85	1.91
	p		1.72	2.81		1.25	2.92
	d	0.23	95.45	94.88	0.07	96.89	95.17
	f	35.15			35.51		
	g	48.66			49.58		
	% charge intersphere		5.46			4.42	
	energy		−0.79442			−2.21099	
	occupancy		2.00			2.00	
$4a_1'$	% charge	1.61	13.25	11.08	0.49	15.72	10.96
	s	98.69	88.51	71.59	96.72	86.95	72.71
	p		7.56	10.94		9.62	14.53
	d	1.11	3.93	17.47	2.39	3.44	12.76
	f	0.19			0.73		
	g	0.01			0.17		
	% charge intersphere		36.47			30.44	
	energy		−0.55739			−1.88216	
	occupancy		2.00			1.00	
$3a_2''$	% charge	8.41	4.27	19.78	3.12	5.01	24.13
	s			99.12			98.65
	p	96.19	74.00	0.25	91.36	78.64	1.27
	d		26.00	0.63		21.36	0.08
	f	3.68			8.43		
	g	0.14			0.21		
	% charge intersphere		39.23			33.60	
	energy		−0.36631			−1.65195	
	occupancy		2.00			0.00	
$6e'$	% charge	8.08	12.27	2.83	2.33	17.06	2.88
	s		82.38			87.14	
	p	96.57	13.58	69.11	91.57	9.98	69.62
	d	2.97	4.05	30.89	7.23	2.88	30.38
	f	0.02			0.00		
	g	0.44			1.20		
	% charge intersphere		49.45			40.73	
	energy		−0.32466			−1.60712	
	occupancy		1.00			0.00	

correct to completely dismiss these levels in any bonding description of these clusters.

Optical Properties. The only definite optical absorptions associated with Ag_5^0 in Ar, Kr, and Xe matrices fall in the range 585–615 nm[10] (listed in Table IV as being centered at 600 nm). Electronic transitions that have been connected with a cationic silver cluster Ag_n^{s+} (n in the range 5–13) entrapped in the supercage of zeolite Y occur at 580, 460, and 390 nm, which shift to 600 and 410 nm on photoreduction to Ag_n^{r+} (the value of n remaining unchanged).[8] In Table IV we list the low-energy dipole-allowed electronic excitations computed from the ground-state spin-restricted Xα molecular orbital energy level scheme of Ag_5^{q+} (q = 0, 2, or 4). In the case of Ag_5^0 it would seem that the HOMO → LUMO $6e' \rightarrow 5a_1'$ excitation calculated around 689 nm is best associated with the lowest energy visible band at 585–615 nm in Ar, Kr, and Xe matrices. Because of the uncertainty in the value of the nuclearity n for the zeolite Y entrapped Ag_n^{s+} and Ag_n^{r+} clusters,[8] it is tenuous at best to propose definite assignments for the observed electronic transitions listed in Table IV by comparison with the cationic Ag_5^{2+} and Ag_5^{4+} clusters of the present study. Nevertheless, it is instructive to examine the trends in the optical spectra as a function of charge depletion for the cases at hand. Interestingly, one observes a blue shift in the energies of the calculated and observed transitions as charge is monotonically removed from the cluster, although, noteably, certain bands became either disallowed or allowed as the valence-electron population of the clusters alters (Table IV).

General EPR Considerations for Ag_5^{4+} and Ag_5^{2+}. The results of the SCF–Xα–SW–MO calculations (Figure 1, Tables I and II) show that the HOMO's of Ag_5^{4+} and Ag_5^{2+} have one electron in each of the Kramer's doublets [$4a_1'\uparrow$; $4a_1'\downarrow$] and [$3a_2''\uparrow$; $3a_2''\downarrow$], respectively. These two clusters are therefore expected to be paramagnetic. The **g** and **A** tensor anisotropies arise from the spin–orbit coupling between the five Ag(k) atomic centers and the unquenching of their orbital angular momenta $l(k)$ via the interaction with the applied magnetic field B. The Hamiltonians representing these two effects are

$$\mathcal{H}_{ls} = \sum_i \sum_k [\zeta(r_k) l_i(k)] s_i \quad (1)$$

$$\mathcal{H}_{lB} = \beta \sum_i \sum_{k'} [l_i(k')] B_i \quad (2)$$

where β is the Bohr magneton and the summations extend over all the atoms of the molecule.

The term $\zeta(r_k)$ is the spin–orbit coupling constant associated with the kth atom. These interactions may be treated as per-

Table IV. Predicted Excitation Energies for the Ag_5^{q+} Molecules (Where q = 0, 2, or 4) and Comparison with Observed Spectra[a]

transition assignment	Ag_5^0		Ag_5^{2+}	Ag_n^{r+}	Ag_5^{4+}	Ag_n^{s+}
	calcd	obsd	calcd	obsd	calcd	obsd
$6e' \rightarrow 7e'$	443		*b*	*b*	*b*	*b*
$6e' \rightarrow 5e''$	463		*b*	*b*	*b*	*b*
$6e' \rightarrow 6a_1'$	477		*b*	*b*	*b*	*b*
$6e' \rightarrow 5a_1'$	689	600	*b*	*b*	*b*	*b*
$3a_2'' \rightarrow 5e''$	382		334		*b*	*b*
$3a_2'' \rightarrow 6a_1'$	392		340		*b*	*b*
$3a_2'' \rightarrow 5a_1'$	524		482		*b*	*b*
$4a_1' \rightarrow 6e'$	392		359	410	331	390
$4a_1' \rightarrow 3a_2''$	*b*	*b*	425	600	396	580
$1a_2'' \rightarrow 4a_1'$	*b*	*b*	*b*	*b*	283	
$1e' \rightarrow 4a_1'$	*b*	*b*	*b*	*b*	295	
$2e' \rightarrow 4a_1'$	*b*	*b*	*b*	*b*	319	
$3e' \rightarrow 4a_1'$	*b*	*b*	*b*	*b*	354	460
$4e' \rightarrow 4a_1'$	*b*	*b*	*b*	*b*	429	
$2a_2'' \rightarrow 4a_1'$	*b*	*b*	*b*	*b*	457	
$5e' \rightarrow 4a_1'$	*b*	*b*	*b*	*b*	461	

[a] All energies are quoted in nanometer units. Note that all predicted energies were calculated as the difference in ground-state eigenvalues. [b] Not allowed.

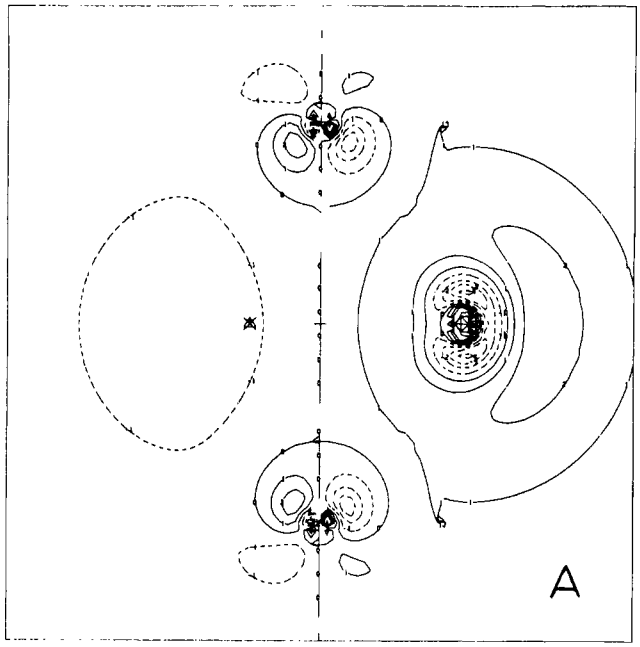

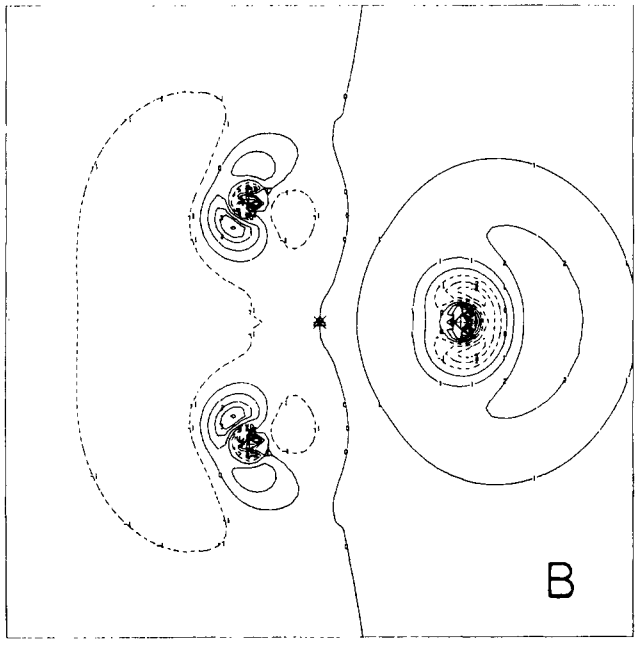

Figure 8. Wave-function contour diagrams for the 6e′ molecular orbital (HOMO) of neutral Ag_5^0. (A) Plot of the xz plane, (B) plot of the xy plane. See Figure 2 caption for contour specifications.

turbants to the original Hamiltonian and thus lead to the second-order corrections:

$$\mathcal{H}_{pert} = \sum_{n\neq 0}\sum_{i,k,k'} \frac{\langle 0|\zeta(k)l_i(k)S_i + \beta l_i(k')B_i|n\rangle\langle n|\zeta(k)l_j(k)S_j + \beta l_j(k')B_j|0\rangle}{\epsilon(n) - \epsilon(0)} \quad (3)$$

Since the Ag_5^{2+} and Ag_5^{4+} clusters have an effective spin of $S = {}^1/_2$, then it is appropriate to neglect the terms containing S_iS_j and B_iB_j in eq 3. This leads to

$$\mathcal{H}_{pert} = \beta \sum_{i,j=x,y,z} \mathbf{g}_{ij}B_iS_j \quad (4)$$

where $\mathbf{g}_{ij}$ is the guage invariant second-rank Cartesian magnetogyric $\mathbf{g}$ tensor given explicitly by

$$\mathbf{g}_{ij} = \mathbf{g}_e\delta_{ij} - 2\sum_{n\neq 0}\sum_{k}\sum_{k'} \frac{\zeta(k)\langle 0|l_i(k)|n\rangle\langle n|l_j(k')|0\rangle}{\epsilon(n) - \epsilon(0)} \quad (5)$$

Table V. Relevant Spatial Symmetry Adapted Linear Combination of Atomic Orbitals

$|na_1'\rangle = N(na_1')\{C_1(na_1')[(1/3^{1/2})[s(2) + s(4) + s(5)]] + C_2(na_1')[1/12^{1/12})[2p_x(2) - p_x(4) - p_x(5)] + {}^1/_2[p_y(4) - p_y(5)]] + C_3(na_1')[(1/3^{1/2})[d_{z^2}(2) + d_{z^2}(4) + d_{z^2}(5)]] + C_4(na_1')[(1/12^{1/2})[2d_{x^2-y^2}(2) - d_{x^2-y^2}(4) - d_{x^2-y^2}(5)] - {}^1/_2[d_{xy}(4) - d_{xy}(5)]] + C_5(na_1')[(1/2^{1/2})[s(3) + s(6)]] + C_6(na_1')[(1/2^{1/2})[p_z(3) - p_z(6)]] + C_7(na_1')[(1/2^{1/2})[d_{z^2}(3) + d_{z^2}(6)]]\}$

$|na_2'\rangle = N(na_2')\{C_1(na_2')[(1/3^{1/2})p_y(2) - {}^1/_2[p_x(4) - p_x(5)] - (1/12^{1/2})[p_y(4) + p_y(5)]] + C_2(na_2')[(1/3^{1/2})d_{xy}(2) + {}^1/_2[d_{x^2-y^2}(4) - d_{x^2-y^2}(5)] - (1/12^{1/2})[d_{xy}(4) + d_{xy}(5)]]\}$

$|na_1''\rangle = N(na_1'')\{C_1(na_1'')[-{}^1/_2[d_{xz}(4) - d_{xz}(5)] + (1/12^{1/2})[2d_{yz}(2) - d_{yz}(4) - d_{yz}(5)]]\}$

$|na_2''\rangle = N(na_2'')\{C_1(na_2'')[(1/3^{1/2})[p_z(2) + p_z(4) + p_z(5)] + C_2(na_2'')[(1/12^{1/2})[2d_{xz}(2) - d_{xz}(4) - d_{xz}(5)] + {}^1/_2[d_{yz}(4) - d_{yz}(5)]] + C_3(na_2'')[(1/2^{1/2})[s(3) - s(6)]] + C_4(na_2'')[1/2^{1/2}[p_z(3) + p_z(6)]] + C_5(na_2'')[(1/2^{1/2})[d_{z^2}(3) - d_{z^2}(6)]]\}$

$|ne''\rangle = N(ne'')\{C_1(ne'')[(1/2^{1/2})[p_z(4) - p_z(5)]] + C_2(ne'')[(1/24^{1/2})[4d_{yz}(2) + d_{yz}(4) + d_{yz}(5)] + (1/8^{1/2})[d_{xz}(4) - d_{xz}(5)]] + C_3(ne'')[(1/8^{1/2})[d_{xz}(4) - d_{xz}(5)] - (3/8)^{1/2}[d_{yz}(4) + d_{yz}(5)]] + [C_4(ne'')/2^{1/2}][p_y(3) - p_y(6)] + [C_5(ne'')/2^{1/2}][d_{yz}(3) + d_{yz}(6)] + [C_6(ne'')/2^{1/2}][d_{xy}(3) - d_{xy}(6)]]\}$

Magnetogyric (g) Tensor for Ag_5^{4+}. In the case of Ag_5^{4+} (Figure 1), the orbitals lying nearest the $|4a_1'\rangle$ HOMO are the $|2a_2''\rangle$, $|4e''\rangle$, $|3e''\rangle$, $|3a_2''\rangle$, and $|5e''\rangle$. Within the approximation used to derive $\mathbf{g}_{ij}$ it is easily seen that only the orbitals transforming as the A_2' and E'' irreducible representations are coupled with the ground-state $|4a_1'\rangle$ orbital leading to anisotropic contributions to the $\mathbf{g}$ tensor. The matrix elements in eq 5 may be determined by the use of the Wigner Eckart theorem and the $3jm$ symbols once the charge distributions for the $|a_2'\rangle$, $|ne_1''\rangle$, and $|ne_2''\rangle$ are known. These orbitals must be expressed in a form that explicitly shows their angular dependence. These take the form of spacial symmetry-adapted linear combinations of atomic orbitals shown in Table V.

In addition to having their angular components normalized, the $N(n)$ factors ensure that the total sum of charge is properly normalized for each one-electron molecular orbital. The use of these wave functions in eq 5 yields zero off-diagonal $\mathbf{g}$-tensor matrix elements. For the $\mathbf{g}_{zz}$ component, which is coincident with the $C_3(z)$ symmetry axis of the molecule, it is found to be

$$\mathbf{g}_{zz} = \mathbf{g}_e - \frac{2\zeta(Ag_2)N^2(4a_1')N^2(1a_2')|C_2(4a_1')C_1(1a_2') + 2C_4(4a_1')C_2(1a_2')|^2}{\epsilon(1a_2') - \epsilon(4a_1')} \quad (6)$$

where Ag_2 denotes the three equatorial silver atoms. The contribution to the anisotropy comes solely from the three equatorial silver centers. This is due to the fact that the $|1a_2'\rangle$ state has no components from the axial silver centers Ag(3) and Ag(6) denoted by Ag_3.

On the other hand the $\mathbf{g}_{xx}$ and $\mathbf{g}_{yy}$ components are equal and are given by:

$$\mathbf{g}_{xx} = \mathbf{g}_{yy} = \mathbf{g}_e - 2\sum_{n=3,4} \frac{[\zeta(Ag_3)A(ne'') + \zeta(Ag_2)B(ne'')][A^*(ne'') + B^*(ne'')]}{\epsilon(ne'') - \epsilon(4a_1')} \quad (7)$$

The explicit expressions for $A(ne'')$ and $B(ne'')$ are

$$A(ne'') = (iN(4a_1')N(ne'')/2^{1/2})\{-C_2^*(4a_1')C_1(ne'') + 3^{1/2}C_3^*(4a_1'')[C_2(ne'') - C_3(ne'')] + C_4^*(4a_1')[C_2(ne'') + C_3(ne')]\} \quad (8)$$

and

$$B(ne'') = iN(4a_1')N(ne'')\{C_6^*(4a_1')C_4(ne'') + 3^{1/2}C_7^*(4a_1') \times [C_5(ne'') + C_6(ne'')]\} \quad (9)$$

Thus as expected the Ag_5^{4+} cluster is predicted to possess an axially symmetric $\mathbf{g}$ tensor. It is to be noted that there are no off-diagonal $\mathbf{g}$ tensor terms, $\mathbf{g}_{ij} = 0$ $(i \neq j)$. This indicates that the principal

axes of the **g** tensor are collinear with the molecular symmetry axes of the cluster.

If the exact values of $\mathbf{g}_{xx}$, $\mathbf{g}_{yy}$, and $\mathbf{g}_{zz}$ are to be theoretically and numerically estimated, all the molecular orbital coefficients and their signs appearing in eq 6–8 must be determined. Our present SCF–Xα–SW algorithm does not possess provisions for explicitly determining all of these coefficients. However, an upper limit on the deviation of the $\mathbf{g}_{ii}$ components from $\mathbf{g}_e$ may be easily estimated utilizing the partial wave analysis for the metal cluster. The partial wave analysis yields the percentage of charge within a certain atomic sphere of the molecule and its distribution among the s, p, and d atomic orbitals. It is thus proportional to the absolute sum of the *squares* of the molecular orbital coefficients of the s, p, and d components within each sphere. If the molecular orbitals have a significant fraction of their charge in the intersphere region of the molecule, then the intersphere charge must be reallocated to its parental atomic spheres. There exists more than one phenomenological method of reallocating the intersphere charge,[6,19] and they are individually suited for the different systems under study. Fortunately, in our particular case, due to the relatively high symmetry of the Ag_5^{n+} clusters and the comparable magnitudes of their sphere radii, a simple reallocation of the intersphere charge that is proportional to the existing charge within each sphere is possible. The resulting redistributed charge for the relevant orbitals is shown in Table VI.

If the signs of the molecular orbital coefficients are chosen so as to maximize the values of the $A(ne'')$ and $B(ne'')$ expressions in eq 8 and 9, then a simple calculation using eq 6 and 7 yields

$$\mathbf{g}_{zz}(\max) = 2.01497$$

$$\mathbf{g}_{xx}(\max) = \mathbf{g}_{yy}(\max) = 2.04670$$

Consequently the maximum difference in the resonance field positions between $\mathbf{g}_{zz}$ and the components $\mathbf{g}_{xx}$ and $\mathbf{g}_{yy}$ at X-band frequencies is estimated to be approximately 53.0 G.

This small **g**-tensor anisotropy is understood by examination of the molecular orbital expressions (Table V) and their corresponding charge distributions (Table VI). The 4e″ and 3e″ orbitals are mainly 4d in character with about 80–90% of the electronic charge shared among the d_{xy}, $d_{x^2-y^2}$, d_{xz}, and d_{yz} atomic orbitals of the axial silver centers. Consequently the coefficients $C_5(ne'')$ and $C_6(ne'')$ are large compared to the rest. In contrast, the $4a_1'$ HOMO is mainly 5s in character and only about 6% of its unpaired electron charge is 4d in character. Thus the molecular orbital coefficients $C_4(4a_1')$, $C_6(4a_1')$, and $C_7(4a_1')$ are small (of the order of 0.1–0.2). In the expression for B, which is the main contributor to $\Delta\mathbf{g}_\perp$, the $C_7(4a_1')$ and $C_5(ne'')$ coefficients are multiplied by one another. Thus, the effect of the large $C_5(ne'')$ is offset by the small $C_7(4a_1')$ and leads to a relatively small deviation of $\mathbf{g}_\perp$ from $\mathbf{g}_e$.

The $\mathbf{g}_{zz}$ anisotropy is entirely due to coupling of the three equatorial Ag centers, 2, 4, and 5. The main contribution to the $\mathbf{g}_{zz}$ anisotropy arises from the coupling of the 4d orbitals of the equatorial silver atoms. The orbitals involved in the coupling are the $4a_1'$ and $1a_2'$ with the $C_4(4a_1')$ and $C_2(1a_2')$ molecular orbital coefficients. There are also possible contributions from the equatorial 5p orbitals. However, from the values of their molecular orbital coefficients, $C_2(4a_1')$ and $C_1(1a_2')$ given in Table VI, their contributions are estimated to be comparitively very small.

Superhyperfine Tensor for Ag_5^{4+}. The hyperfine interaction of the unpaired electron with the Ag nuclei may be expressed in the following way

$$\mathcal{H}_{\text{hyp}} = \frac{\mathbf{g}_e\beta\beta_N}{\langle r^3\rangle}\sum_{i=2}^{6}\mathbf{g}_N(\text{Ag}_i)\Big\{[I(\text{Ag}_i)\cdot S + 3(r_i\cdot I(\text{Ag}_i)) \times (r_i\cdot S)] + \frac{8\pi}{3}|\Psi(r_i)|^2\delta(r_i)S\cdot I(\text{Ag}_1)\Big\} \quad (10)$$

where β_N and $I(\text{Ag}_i)$ are the nuclear magneton and spin operator of the ith Ag nucleus. The first component in eq 10 is the anisotropic dipole–nuclear dipole interaction, while the second component represents the isotropic Fermi contact term. In a gauge invariant molecular orbital representation the anisotropic component of the hyperfine interaction takes the form[20]

$$A_{vw} = \mathbf{g}\beta\mathbf{g}_N\beta_N\Big\{\Big\langle\psi_n\Big|\frac{F_{vw}}{r^3}\Big|\psi_n\Big\rangle + \sum_{m\neq 0}\frac{1}{\epsilon(m)-\epsilon(n)}\sum_{k'}\Big(2\langle\psi_n|\zeta(k')l_v(k')|\psi_m\rangle \times \Big\langle\psi_m\Big|\frac{l_w}{r^3}\Big|\psi_n\Big\rangle + i\sum_u\sum_t\epsilon_{utv}\langle\psi_n|\zeta(k')l_u(k')|\psi_m\rangle\Big\langle\psi_m\Big|\frac{F_{tw}}{r^3}\Big|\psi_n\Big\rangle\Big)\Big\} \quad (11)$$

where ϵ_{utv} is the Levi–Civita antisymmetric third-rank unit tensor.

Table VI. Ground- and Excited-State Charge Distributions after Charge Reallocation

atoms		GS	ES
	Ag_5^{2+} HOMO $3a_2''$		
2,4,5	% p	0.192 11	
	% d	0.056 11	
3,6	% s	0.743 48	
	% p	0.000 60	
	% d	0.002 68	
	Ag_5^{2+} HOMO $1a''$		
2,4,5	% d	1.000 00	1.000 0
	Ag_5^{2+} HOMO $4e'$		
2,4,5	% s	0.000 05	0.000 45
	% p	0.000 09	0.000 10
	% d	0.018 56	0.196 79
3,6	% p	0.000 01	0.000 00
	% d	0.980 40	0.802 65
	Ag_5^{2+} HOMO $5e'$		
2,4,5	% s	0.004 92	0.001 68
	% p	0.000 71	0.000 49
	% d	0.216 29	0.375 93
3,6	% p	0.000 43	0.000 96
	% d	0.777 66	0.620 94
	Ag_5^{2+} HOMO $6e'$		
2,4,5	% s	0.747 48	0.743 42
	% p	0.104 05	0.104 84
	% d	0.029 83	0.032 41
3,6	% p	0.079 42	0.086 94
	% d	0.039 22	0.032 41
	Ag_5^{2+} HOMO $7e'$		
2,4,5	% s	0.153 24	0.158 44
	% p	0.769 47	0.762 33
	% d	0.010 84	0.010 68
3,6	% p	0.036 71	0.040 94
	% d	0.029 75	0.027 62
	Ag_5^{4+} HOMO $4a_1'$		
2,4,5	% s	0.593 57	
	% p	0.065 62	
	% d	0.023 47	
3,6	% s	0.230 76	
	% p	0.046 09	
	% d	0.040 49	
	Ag_5^{4+} HOMO $1a_2'$		
2,4,5	% p	0.002 84	0.002 45
	% d	0.997 16	0.997 55
	Ag_5^{4+} HOMO $4e'$		
2,4,5	% p	0.004 68	0.003 44
	% d	0.188 42	0.468 34
3,6	% p	0.000 19	0.000 56
	% d	0.806 71	0.527 66
	Ag_5^{4+} HOMO $3e''$		
2,4,5	% p	0.001 13	0.000 18
	% d	0.059 67	0.443 88
3,6	% p	0.000 01	0.000 07
	% d	0.939 20	0.555 87

(19) Case, D. A.; Karplus, M. *Chem. Phys. Lett.* **1976**, *39*, 33.

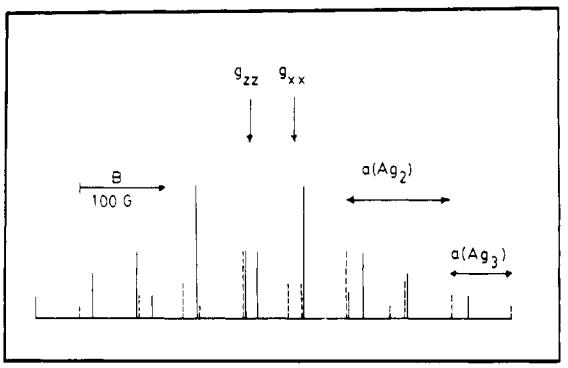

Figure 9. Predicted EPR powder stick spectrum of isotopically pure $^{109}Ag_5^{4+}$ at X-band frequencies (assuming the free electron resonates at 3400 G). The parallel components of the spectrum are represented by dashed lines, whereas the perpendicular components are shown as solid lines (see text for details).

All the remaining symbols in eq 11 have been described previously.[20]

For the Ag_5^{4+} cluster the $4a_1'$ orbital is estimated to be approximately 82.5% 5s in character. Consequently the effects of the anisotropic components will not be large and are not expected to yield resolved splittings. However, such anisotropies are expected to manifest themselves as additional broading of the spectral line shapes. It is thus assumed that the hyperfine splitting arises only from the isotropic Fermi contact term. The values of the isotropic hyperfine splitting of nucleus Ag_i is proportional to the unpaired electron charge density at the nucleus. In a nonspin polarized (spin restricted) calculation this is proportional to the percentage s character of the $4a_1'$ orbital at this nucleus. Since core polarization effects are usually difficult to estimate, for our present purposes, the magnitude of the isotropic splitting is estimated using the following method. For the free Ag atom, in the gas phase, the unpaired electron resides entirely in the 5s orbital. The measured isotropic hyperfine tensor is 613.0 G.[21] It is assumed that the isotropic hyperfine splitting is directly proportional to the charge density of the unpaired electron for the sphere containing the Ag nucleus. Consequently, from Table VI the magnitude of the hyperfine components is estimated to be

$$\mathbf{a}^{iso}(2,4,5) = 121.287 \text{ G}$$

and

$$\mathbf{a}^{iso}(3,6) = 70.730 \text{ G}$$

These values, together with those of $\mathbf{g}_{xx}$, $\mathbf{g}_{yy}$, and $\mathbf{g}_{zz}$ are utilized to construct the hypothetical powder stick spectrum shown in Figure 9. The Xα–MS–MO calculation predicts two quartets centered around $g_{xx} = g_{yy}$ and g_{zz}. Each line of the quartets is separated by 121.29 G. Each line is further split into a triplet whose lines are separated by 70.73 G leading to a total of 24 lines.

Magnetogyric (g) Tensor for Ag_5^{2+}. In the case of the Ag_5^{2+} cluster the $3a_2''$ orbital is the HOMO and it contains one electron. The molecular orbitals that couple with the $3a_2''$ to cause the $\mathbf{g}_{zz}$ tensor components to deviate from $\mathbf{g}_e$ are those of a_1'' symmetry. Thus, by using eq 6 $\mathbf{g}_{zz}$ is found to be

$$\mathbf{g}_{zz} = \mathbf{g}_e - 2\zeta(Ag_2)\frac{|N(1a_1'')N(3a_2'')C_1(1a_1'')C_2(3a_2'')|^2}{\epsilon(1a_1'') - \epsilon(3a_2'')} \quad (12)$$

and is numerically estimated to be extremely close to the value of $\mathbf{g}_e = 2.0023$. This is because the $\mathbf{g}_{zz}$ anisotropy arises from the coupling of the d character of axial silver atoms in the $3a_2''$ and $1a_1''$ states. The energy separation, calculated by the transition state method, for these levels is quite large (51 459.38 cm^{-1}). In addition only about 2.2×10^{-3} of the total charge density of the $3a_2''$ orbital is attributable to d-character components of the axial silver atoms. These two factors render the $\mathbf{g}_{zz}$ anisotropy practically insignificant ($\Delta\mathbf{g}_{zz} = 4.0 \times 10^{-6}$). Again as for the Ag_5^{4+} cluster, all off-diagonal **g** tensor elements are found to be zero. However, $\mathbf{g}_{xx}$ is equal to $\mathbf{g}_{yy}$ and their anisotropy arises from the admixtures of the $3a_2''$ orbital with orbitals of e' symmetry. The energy difference between the $3a_2''$ and the 4e', 5e', 6e', and 7e' orbitals are found, from transition-state calculations, to be approximately 44 500, 40 378, 4700, and 31 307 cm^{-1}, respectively. Energy separations greater than 45 000 cm^{-1} are considered large and the contribution of their corresponding orbitals to $\mathbf{g}_{xx}$ and $\mathbf{g}_{yy}$ may be neglected. Consequently,

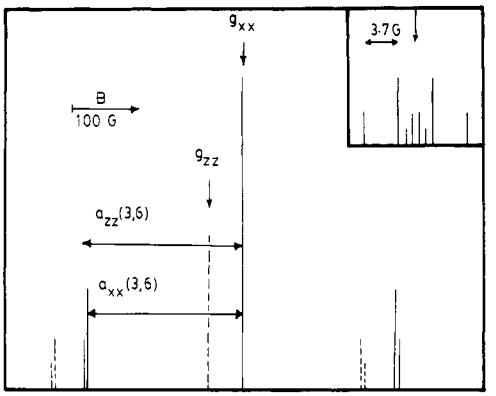

Figure 10. Predicted EPR powder stick spectrum of isotopically pure $^{109}Ag_5^{2+}$ with the same parameters and notation as used in Figure 9. In addition, every one of the 10 main resonance lines in the principal spectrum is further split into two quartets as shown in the inset of the Figure (see text for details).

$$\mathbf{g}_{xx} = \mathbf{g}_{yy} = \mathbf{g}_e - 2\sum_{n=4}^{7}\zeta(Ag_2)\frac{|A(n) + B(n)|^2}{\epsilon(ne') - \epsilon(3a_2'')} \quad (13)$$

where in this case, $A(n)$ and $B(n)$ are given by

$$A(n) = N(3a_2'')N(ne')i2^{1/2}\{C_1^*(3a_2'')[C_2(ne') + C_3(ne')] + C_2^*(3a_2'')[-3^{1/2}C_4(ne') + C_5(ne') - C_6(ne')]\} \quad (14)$$

and

$$B(n) = N(3a_2'')N(ne')i[C_4^*(3a_2'')C_7(ne') + 3^{1/2}C_5^*(3a_2'')C_8(ne')] \quad (15)$$

The reallocation of outer sphere and intersphere charge followed by the substitution of the molecular orbital coefficients yields the maximum values of $\mathbf{g}_{xx}$ and $\mathbf{g}_{yy}$ (vide infra) as

$$\mathbf{g}_{xx}(\max) = \mathbf{g}_{yy}(\max) = 1.9713$$

Examination of the charge distribution of the $3a_2''$ orbital (Table VI) unveils that most of its unpaired electron charge density resides on the 5s atomic orbitals of the axial Ag_3 atoms. The 5s components do not couple with the *ne'* orbitals via orbital angular momentum and hence do not contribute to the anisotropy of the **g** tensor components. The remaining charge density of the $3a_2''$ (19.2%) is mainly situated on the $5p_x$ and $5p_y$ of the equatorial Ag_2 centers. Thus any contribution to $\mathbf{g}_{xx}$ and $\mathbf{g}_{yy}$ must mainly involve the p character of the e' orbitals. The contribution of the filled 4e' and 5e' orbitals to $\mathbf{g}_{xx}$ and $\mathbf{g}_{yy}$ is cancelled by the unoccupied 7e' orbital that has a larger p (76.9%) character. Thus the net anisotropy of the $\mathbf{g}_{xx}$ and $\mathbf{g}_{yy}$ components may be envisaged as almost entirely due to the coupling of the $3a_2''$ with the 6e' orbital. Although the 6e' has only 10.4% of its charge density that is p in character its close proximity to the $3a_2''$ HOMO (4700 cm^{-1}) renders its contribution to the **g** anisotropy relatively quite large.

Superhyperfine Tensors for Ag_5^{2+}. The hyperfine splitting pattern for the Ag_5^{2+} cluster will be very different from that of the Ag_5^{4+} cluster derived earlier. The $3a_2''$ HOMO as dictated by symmetry, contains no 5s character arising from the equatorial Ag_2 centers. Hence to a first approximation there exists no equatorial isotropic hyperfine splittings. By employing similar

(20) Keijzers, C. P.; De Boer, E. *J. Chem. Phys.* **1972**, *57*, 1279.
(21) Kasai, P. H.; McLeod, Jr., D. *J. Chem. Phys.* **1971**, *55*, 1566.

$$a^{\text{aniso}}(2,4,5) = \frac{g_e\beta g_N\beta_N}{\langle r^3\rangle} \times$$

$$\begin{bmatrix} \frac{2}{15}N^2(3a_2'')C_1^2(3a_2'') & & \\ \frac{2}{3^{1/2}}\sum_{n=1}^{7}\frac{\zeta(Ag_2)[A(n)+B(n)]A^*(n)}{\epsilon(ne')-\epsilon(3a_2'')} & 0 & \\ 0 & -\frac{2}{15}N^2(3a_2'')C_1^2(3a_2'') & 0 \\ & -\frac{2}{3^{1/2}}\sum_{n=4}^{7}\frac{\zeta(Ag_2)[A(n)+B(n)]A^*(n)}{\epsilon(ne')-\epsilon(3a_2'')} & 0 \\ 0 & 0 & \frac{4}{15}N^2(3a_2'')C_1^2(3a_2'') - \frac{\Delta g_{zz}}{3} \end{bmatrix} \quad (16)$$

$$a^{\text{aniso}}(3,6) = \frac{g\beta g_N\beta_N}{\langle r^3\rangle} \times$$

$$\begin{bmatrix} \frac{N^2}{2}(3a_2'')\left\{-{}^2/_5C_4^2(3a_2'') - {}^2/_5C_5^2(3a_2'') - \frac{1}{5^{1/2}}[C_3(3a_2'')C_5(3a_2'')] - \right. & 0 & 0 \\ \left. \sum_{n=4}^{7}\frac{\zeta(Ag_2)[A(n)+B(n)]B^*(n)}{\epsilon(ne')-\epsilon(3a_2'')}\right\} & & \\ 0 & \frac{N^2}{2}(3a_2'')\left\{-{}^2/_5C_4^2(3a_2'') - {}^2/_7C_5^2(3a_2'') - \right. & 0 \\ & \left. \frac{1}{5^{1/2}}[C_3(3a_2'')C_5(3a_2'')] - \sum_{n=4}^{7}\frac{\zeta(Ag_2)[A(n)+B(n)]B^*(n)}{\epsilon(ne')-\epsilon(3a_2'')}\right\} & \\ 0 & 0 & \frac{N^2}{2}(3a_2'')\left\{{}^4/_5C_4^2(3a_2'') + \right. \\ & & \left. {}^4/_7C_5^2(3a_2'') + \frac{2}{5^{1/2}}[C_3(3a_2'')C_5(3a)_2)] - \frac{\Delta g_{zz}}{2}\right. \end{bmatrix} \quad (17)$$

methods to those described for Ag_5^{4+} (vide infra), the triplet isotropic hyperfine splitting arising from the two axial silver centers is estimated to be roughly 227.88 G.

Although there are no isotropic hyperfine splittings from the equatorial silver atoms, their anisotropic tensor components are not necessarily zero. For the sake of simplicity, by neglecting the last term in eq 11 together with the equatorial silver atom 4d contributions to the molecular orbitals, one obtains the approximate form of the anisotropic hyperfine tensor for the three equatorial silver centers (eq 16). By use of the numerical values of $|N(3a_2'')C_1(3a_2'')|^2$ from Table VI and $(g_e g_N\beta\beta_N/\langle r^3\rangle)$, and total hyperfine interaction constant for the 2, 4, and 5 Ag centers of Ag_5^{2+} is predicted to be

$$\mathbf{a}_{xx}(2,4,5) = -0.7248 \text{ G} \qquad \mathbf{a}_{yy}(2,4,5) = -0.7248 \text{ G}$$
$$\mathbf{a}_{zz}(2,4,5) = 3.731 \text{ G} \qquad \mathbf{a}_{ij}(2,4,5) = \mathbf{a}_{ji}(2,4,5) = 0$$

where $i,j = x,y,z$ and $i \neq j$. The traces of the equatorial hyperfine tensors in eq 16 are seen not to be zero. This originates from the contributions of the second-order effects arising from the unquenching of orbital angular momentum and spin–orbit coupling.

For the two axial Ag centers 3 and 6 the anisotropic hyperfine tensor components take the more complicated form (eq 17), which numerically yields

$$\mathbf{a}_{xx}(3,6) = 227.48 \text{ G} \qquad \mathbf{a}_{yy}(3,6) = 227.48 \text{ G}$$
$$\mathbf{a}_{zz}(3,6) = 228.08 \text{ G}$$

where $\mathbf{a}_{ij}(3,6) = 0$ for $i,j = x,y,z$ and $i \neq j$. For both the Ag_5^{2+} and Ag_5^{4+} clusters the principal axes of the electronic **g** and nuclear hyperfine tensors are to a first approximation coincident. This result is very helpful and greatly simplifies the procedure of computer simulation of the predicted EPR spectra. The calculated powder stick spectrum for the Ag_5^{2+} cluster is shown in Figure 10.

The Ag_5^{2+} hyperfine tensors for the three spatially equivalent equatorial silver atoms are all the same, rendering them also magnetically equivalent. However, if the contributions from the d_{xz} and d_{yz} (although small) atomic orbitals for these atoms were included in estimating **a**(2,4,5), then the tensor components would be different leading to magnetic inequivalency for the three equatorial silver centers. This is because for a particular center the superhyperfine tensors reflect the symmetry of the local electronic distribution at that center which is not necessarily the point symmetry of the molecule, in this case D_{3h}.

General Discussion

The derivation of the effective spin Hamiltonian tensor components from the theoretically computed wave functions invoked a small spin–orbit interaction. Consequently this interaction could be handled by means of perturbation techniques as applied to the electronic ground-state wave functions. Rigorously, however, the admixture of higher excited states with the ground state appearing in the matrix elements of eq 6 should make use of excited-state wave functions and charge distributions.[22] The difference in charge distribution between the molecule when in its ground and excited states and its effect on the EPR spin Hamiltonian tensor components has not been investigated in detail previously. Table VI lists the charge distributions of some relevant molecular orbitals in both the ground and excited electronic states. One finds that the charge distribution of some molecular orbitals is rather insensitive to whether they contain one electron more or less than

(22) Smith, D. W. *J. Chem. Soc. A* **1970**, 3108. McGarvey, B., personal communication.

the ground-state configuration. On the other hand, some molecular orbitals display drastic alterations in their spacial charge distribution on passing from a ground to an excited electronic state configuration. For the Ag_5^{2+} and Ag_5^{4+} clusters, these molecular orbitals are the filled e′ and e″ states. Their charge distribution changes significantly when an electron is excited from these orbitals to a HOMO as illustrated in Table VI. Consequently, the use of charge distributions for the e″ and e′ in the ground and excited states yields different values for the $\mathbf{g}_{xx}$ and $\mathbf{g}_{yy}$ components in the Ag_5^{n+} clusters. Thus extreme caution must be exercised in cases similar to those described above, when utilizing charge distributions of molecular orbitals obtained from ground-state calculations. The appropriate excited states should be computed and their resulting charge distributions used in numerical estimations of the spin Hamiltonian **g** tensor components. Finally, one should note that, in all of our calculations of EPR parameters, the energy differences occurring in the denominator of eq 6 were estimated by the Slater transition-state procedure.[3,12]

Conclusion

The SCF-Xα-SW-MO method has been used to calculate the ground- and excited-state wave functions, charge distributions, and molecular orbital energies of trigonal-bipyramidal isotopically pure $^{109}Ag_5^{q+}$ clusters (q = 0-4). One goal of this study was to gain an insight into the effect of gradually depleting valence electronic charge from the neutral parent cluster Ag_5^0 on the electronic and magnetic properties of the resulting cationic Ag_5^{q+} clusters. The problem was approached by calculating the optical transition energies and EPR spin Hamiltonian tensor components for selected Ag_5^{q+} clusters. In the case of their optical spectra, significant changes were predicted on passing from Ag_5^0 to Ag_5^{2+} to Ag_5^{4+}. Specifically, certain dipole-allowed transitions found for one cluster were not allowed for another. Also, transitions that were common to two, or all three clusters, were predicted to blue shift with increasing positive charge on the cluster. This behavior paralleled the monotonic relaxation of all molecular orbital levels with increasing positive charge on the cluster. Trends of this type are expected to be important when attempting to analyze optical absorption, reflectance, or fluorescence spectra of neutral and/or cationic silver clusters entrapped in, for example, rare gas solid, zeolite, or aqueous glassy matrices.

The electronic ground states of these pentaatomic silver clusters are also found to change on passing from Ag_5^0 ($^2E'$) to Ag_5^{2+} ($^2A_1'$) to Ag_5^{4+} ($^2A_2''$). This is found to have a dramatic effect on their predicted magnetogyric **g** tensor components and hyperfine-splitting patterns. In the case of Ag_5^{4+}, the calculated EPR spectrum comprises essentially an isotropic set of quartets whose lines are separated by 121.287 G and are centered aroung $\mathbf{g}_{zz}$ = 2.01497 and $\mathbf{g}_{xx} = \mathbf{g}_{yy}$ = 2.04670, arising from coupling of the unpaired electron with three magnetically equivalent equatorial silver centers. Each line is further split into a triplet by coupling to two similarly equivalent axial silver centers whose lines are separated by 70.73 G, thereby yielding a 24-line hyperfine pattern (Figure 9). This spectrum is quite distinct from the EPR spectrum predicted for Ag_5^{2+}. The latter is best described as a set of two triplets centered around $\mathbf{g}_{xx} = \mathbf{g}_{yy}$ = 1.9713 and split by 228.08 and 227.48. The two center lines of these triplets coincide with one another, thus leading to apparently five resonances (Figure 10). A similar splitting pattern exists for the $\mathbf{g}_{zz}$ = 2.0023. Thus the superhyperfine splitting from the axial silver centers is predicted to yield 10 resonance lines. When the parallel and perpendicular components of the equatorial silver superhyperfine tensors are taken into account, every one of the 10 resonances is further split into two quartets with 0.7248 and 3.7 G splittings. Consequently one predicts an 80-line powder stick spectrum as shown in Figure 10.

Acknowledgment. The generous financial assistance of the Natural Sciences and Engineering Research Council of Canada's Operating and Strategic Grants Programmes and the Connaught Foundation of the University of Toronto are both gratefully acknowledged.

Registry No. Ag_5, 64475-46-3.

Unusual Macrocyclic Biphenyls Containing the Dihydropyrene Nucleus. An Observation of Aryl Group Transfer from Phosphine to Aryl Halide Using Nickel Complexes[1]

Reginald H. Mitchell,* Mahima Chaudhary, Thomas W. Dingle, and Richard Vaughan Williams

Contribution from the Department of Chemistry, University of Victoria, Victoria, British Columbia, Canada V8W 2Y2. *Received May 14, 1984*

Abstract: Coupling of 2-bromo-*trans*-10b,10c-dimethyl-10b,10c-dihydropyrene (**5**) by using bis(triphenylphosphino)nickel(II) chloride yielded not only the expected biaryl **2** but also the phenyldihydropyrene **3**. The latter must have arisen through an aryl transfer from the phosphine ligand. The UV and ^1H NMR spectra of **2** and **3** are discussed relative to those of **4** and biphenyl and analyzed with respect to calculated π-SCF bond orders of these molecules. Reduction in ring current of **2** and **3** relative to **4** is minimal, whereas substantial inter-ring interaction is indicated by UV spectroscopy.

Biphenyls have been of interest to organic chemists for more than half a century because of their interesting stereochemistry.[2] More recently a huge amount of synthetic effort appears to have been made to develop efficient aryl coupling methods,[3] which in

(1) Benzannelated Annulenes. 10. For part 9 see: Mitchell, R. H.; Williams, R. V.; Mahadevan, R.; Lai, Y. H.; Dingle, T. W. *J. Am. Chem. Soc.* **1982**, *104*, 2571-2578.

(2) For reviews see: (a) Adams, R.; Yuan, H. C. *Chem. Rev.* **1933**, *12*, 261-338. (b) Hall, D. M. "Progress in Stereochemistry"; Aylett, B. J., Harris, M. W., Eds.; Butterworths: London, 1969; Vol. 4, p 1.

0002-7863/84/1506-7776$01.50/0